The Astrophysical Journal, 580:L11–L15, 2002 November 20

EVIDENCE FOR TIDAL STRIPPING OF DARK MATTER HALOS IN MASSIVE CLUSTER LENSES

Priyamvada Natarajan,[1] Jean-Paul Kneib,[2] and Ian Smail[3]
Received 2002 June 10; accepted 2002 October 4; published 2002 October 23

ABSTRACT

In this Letter, we present the results of our study of galaxy-galaxy lensing in massive cluster lenses spanning $z = 0.17$–0.58, utilizing high-quality archival *Hubble Space Telescope* data. Local anisotropies in the shear maps are assumed to arise from dark matter substructure within these clusters. Associating the substructure with bright early-type cluster galaxies, we quantify the properties of typical L^* cluster members in a statistical fashion. The fraction of total mass associated with individual galaxies within the inner regions of these clusters ranges from 10% to 20%, implying that the bulk of the dark matter in massive lensing clusters is smoothly distributed. Looking at the properties of the cluster galaxies, we find strong evidence (>3 σ significance) that a fiducial early-type L^* galaxy in these clusters has a mass distribution that is tidally truncated compared with equivalent luminosity galaxies in the field. In fact, we exclude field galaxy scale dark halos for these cluster early types at greater than 10 σ significance. We compare the tidal radii obtained from this lensing analysis with the central density of the cluster potentials and find a correlation that is in excellent agreement with theoretical expectations of tidal truncation: $\log r_t^* \propto (-0.6 \pm 0.2) \log \rho_0$.

Subject headings: galaxies: fundamental parameters — galaxies: halos — gravitational lensing — methods: numerical

1. INTRODUCTION

Galaxy-galaxy lensing provides a powerful tool for statistically measuring the mass distribution for field galaxies (Tyson et al. 1984; Brainerd, Blandford, & Smail 1996). These studies confirm the existence of massive dark matter halos around typical field galaxies, extending to beyond 100 kpc (Brainerd et al. 1996; Fischer et al. 2000; Smith et al. 2001a; McKay et al. 2001).[4] The same technique can be modified and implemented within clusters to constrain the masses of cluster galaxies (Natarajan & Kneib 1997, hereafter NK97; Geiger & Schneider 1998). The successful application of this technique to the rich lensing cluster AC 114 at $z = 0.31$ suggests that the average M/L ratio and spatial extents of the dark matter halos associated with early-type galaxies in such dense environments may differ from those of comparable luminosity field galaxies (Natarajan et al. 1998, hereafter NKSE98).

The technique applied by NKSE98 quantifies the local weak distortions in the observed shear field of massive cluster lenses as perturbations arising from the massive halos of cluster galaxies (for details, see NK97). By associating these perturbations with bright early-type cluster members, the relative mass fraction in their halos is constrained using a combined χ^2 maximum likelihood method. The strength of this approach is the simultaneous use of constraints from the observed strong and weak lensing features.

The fractional mass in clusters associated with individual galaxy halos has important consequences for the frequency and nature of interactions (Moore et al. 1996; Ghigna et al. 1998; Okamato & Habe 1999; Merritt 1983). The theoretical expectation is that the global tidal field of a massive, dense cluster potential well should be strong enough to truncate the dark matter halos of galaxies that traverse the cluster core. In this Letter, we test this expectation using well-calibrated mass models for rich clusters at $z \sim 0.17$–0.58 that utilize the observed strong lensing features—positions, magnitudes, geometry of multiple images, measured spectroscopic redshifts, as well as the shear field.

2. GALAXY-GALAXY LENSING IN CLUSTERS

The clusters in our study are modeled as a superposition of a smooth large-scale potential and smaller scale potentials that are associated with bright early-type cluster members: $\phi_{\rm tot} = \phi_{\rm clus} + \Sigma_i \phi_{p_i}$, where $\phi_{\rm clus}$ is the potential of the smooth component and ϕ_{p_i} are the potentials of the perturbers (galaxy halos).[5]

To quantify the lensing distortion induced by $\phi_{\rm tot}$, the smooth cluster piece and individual galaxy-scale halos are modeled self-similarly using the pseudoisothermal elliptical surface density profile $\Sigma(R)$ derived by Kassiola & Kovner (1993), with a core radius r_0, a truncation radius $r_t \gg r_0$, and an ellipticity ϵ. These parameters are tuned for both the smooth component and the perturbers to obtain mass distributions on the relevant scales (for details, see § 2.2 of NK97). Note that r_t characterizes the scale over which the local potential dominates. Additionally, assuming light traces mass, the light distribution of the early-type cluster members is related to the mass model via a set of the usual adopted scaling laws motivated by observations (see Brainerd et al. 1996):

$$\sigma_0 = \sigma_* \left(\frac{L}{L_*}\right)^{1/4}; \quad r_0 = r_0^* \left(\frac{L}{L_*}\right)^{1/2}; \quad r_t = r_t^* \left(\frac{L}{L_*}\right)^{1/2}. \quad (1)$$

The effect of these assumed scaling laws on the maximum likelihood analysis has been explored in detail using simulations in NK97. The total mass M and the total mass-to-light

[1] Department of Astronomy, Yale University, 260 Whitney Avenue, New Haven, CT 06511.

[2] Observatoire Midi-Pyrenees, 14 Avenue Edouard Belin, F-31400 Toulouse, France.

[3] Department of Physics, University of Durham, South Road, Durham DH1 3LE, UK.

[4] We adopt $h = H_0/100$ km s^{-1} Mpc$^{-1} = 0.5$, $q_0 = 0.5$, and $\Omega_0 = 1$. Our results, however, are not sensitive to values of the cosmological parameters.

[5] The reduced shear g, a complex number, is defined in terms of the convergence κ and the shear γ, as $g = \gamma/(1 - \kappa)$, and can be directly related to the measured shape parameter $\tau = 2g/(1 - g^* g)$.

TABLE 1
CLUSTER PROPERTIES

Cluster	z	L_X ($\times 10^{44}$ ergs s^{-1})	T_{exp} (ks)	σ^* (km s^{-1})	r_t^* (kpc)	M_{ap}/L_v ($M_\odot/L_\odot$)	M^* ($\times 10^{11}\ M_\odot$)	σ_{clus} (km s^{-1})	r_c (kpc)	$\rho_{clus}(r_c)$ ($\times 10^6\ M_\odot$ kpc^{-3})
A2218	0.17	9.5	6.3	180 ± 10	40 ± 12	5.8 ± 1.5	~14	1070 ± 70	75 ± 10	3.95
A2390	0.23	23.4	10.5	200 ± 15	18 ± 5	4.2 ± 1.3	~6.4	1100 ± 80	55 ± 10	16.95
AC 114	0.31	13.4	16.8	192 ± 35	17 ± 5	6.2 ± 1.4	~4.9	950 ± 50	45 ± 15	9.12
Cl 2244−02	0.33	4.8	10.5	110 ± 7	55 ± 12	3.2 ± 1.2	~6.8	600 ± 80	30 ± 15	3.52
Cl 0024+16	0.39	2.4	13.2	125 ± 7	45 ± 5	2.5 ± 1.2	~6.3	1000 ± 70	30 ± 10	3.63
Cl 0054−27	0.58	0.25	16.8	230 ± 18	20 ± 7	5.2 ± 1.4	~9.4	1100 ± 100	30 ± 10	15.84

ratio M/L of cluster galaxies then scales as follows:

$$M \propto \sigma_*^2 r_t^* \left(\frac{L}{L_*}\right); \quad \frac{M}{L} \propto \sigma_*^2 r_t^*. \tag{2}$$

The ellipticity of the mass clumps is set to the observed ellipticity of each cluster galaxy. Since we are sensitive to the induced local shear arising as a result of the integrated mass within r_t for the clumps, we are not sensitive to details of the assumed radial falloff or the assumed inner slope of the profile in the galaxy model.

The measured local shear signal in the cluster at the location of the ith perturber is boosted in value because of the contribution from both the shear and the convergence of the smooth cluster component. By taking into account a smooth cluster model, it is possible to reduce the error in the measured shear from the cluster members:

$$\langle g_I - g_c \rangle = \left\langle \frac{\gamma_{p_i}}{1 - \kappa_c - \kappa_{p_i}} \right\rangle, \quad (\sigma^2_{g_I - g_c}) = \frac{\sigma^2_{g_S}}{2} \approx \frac{\sigma^2_{p(\tau_S)}}{N_{bg}},$$

where g_I, g_S, and g_c are the shapes of the lensed image (I), unlensed source (S), and the shear of the smooth cluster piece (c), respectively; $\sigma^2_{p(\tau_S)} \sim 0.3$ is the width of the intrinsic ellipticity distribution of the sources; and N_{bg} is the number of background galaxies averaged over. Therefore, knowledge of a well-calibrated strong lensing model makes the study of galaxy-galaxy lensing in clusters very viable.

A maximum likelihood method is used to obtain significance bounds on fiducial parameters that characterize a typical L^* halo in the cluster. We have extended the formalism developed in NK97 to include the strong lensing data for the inner regions of the clusters; these are used to obtain the best model χ^2 fit followed by a likelihood method that incorporates the constraints from the smoothed shear field.

The likelihood function of the estimated probability distribution of the source ellipticities is maximized for a set of model parameters, given a functional form of the intrinsic ellipticity distribution measured for faint galaxies. The entire inversion procedure to solve the lensing equation is performed for each cluster within the LENSTOOL utilities.[6] Using a well-determined "strong lensing" model for the inner regions of the clusters, along with the averaged shear field, and assuming a known functional form for $p(\tau_S)$ from the field, the likelihood for an estimated model is computed using $\tau_{S_j} = \tau_{\mathrm{obs}_j} - \Sigma_i^{N_c} \gamma_{p_i} - \gamma_c$ for each faint galaxy j, where $\Sigma_i^{N_c} \gamma_{p_i}$ is the sum of the shear contribution from N_c perturbers and γ_c is the shear induced by the smooth component:

$$\mathcal{L}(\sigma_*, r_t^*) = \Pi_j^{N_{gal}} p(\tau_{S_j}). \tag{3}$$

We compute $\mathcal{L}$ by assigning the median redshift corresponding to the observed source magnitude for each arclet (details of this procedure can be found in NK97). The best-fitting model parameters are then obtained by maximizing the log likelihood function l with respect to the chosen set of model parameters (σ_*, r_t^*), and the cluster parameters are simultaneously matched in an iterative way.

3. THE *HUBBLE SPACE TELESCOPE* CLUSTER LENSES

For our analysis, we select clusters at $z > 0.1$ for which deep, high-quality *Hubble Space Telescope* (*HST*) imaging is available and that contain spectroscopically confirmed multiply imaged high-redshift galaxies. These lensed features are essential for constructing a detailed mass distribution for the cluster cores (e.g., Kneib et al. 1996; Smith et al. 2001b), while the existence of spectroscopic redshifts allows us to calibrate these mass distributions onto an absolute scale. This selection yields five clusters with redshifts spanning $z = 0.17$–0.58 for our analysis: A2218, A2390, Cl 2244−02, Cl 0024+16, and Cl 0054−27. In addition to these five clusters, we also include our previous analysis of the $z = 0.31$ cluster AC 114 (NKSE98). Details of the cluster properties are given in Table 1. Clearly, these clusters do not constitute a well-defined sample; for example, their X-ray luminosities span an order of magnitude, and their central mass densities show a similarly large dispersion. It is this latter property that is most interesting for our analysis, and the large range spanned by the sample therefore provides a powerful test of the variations in characteristics of galaxy halos with the local environment.

The five new clusters were observed with the Wide Field Planetary Camera 2 (WFPC2), A2390, Cl 2244−02, Cl 0024+16, and Cl 0054−27 through the F814W (I) passband and A2218 through the F702W (R) passband; the total exposure times are listed in Table 1. These typically comprise stacks of multiple single-orbit (2.1–2.7 ks) exposures, each of which is spatially offset by an integer number of WFC pixels to allow the removal of cosmic rays and other artifacts. The data were pipeline-processed by STScI and combined using standard STSDAS and IRAF routines. For more details of the reduction, see Kneib et al. (1996; A2218); Altieri et al. (1999; A2390), and Smail et al. (1997; Cl 0024+16 and Cl 0054−27). These fields reach typical 5 σ detection limits for point sources of $I \sim 26$ or $R \sim 26.5$.

Object catalogs and attendant shape information for faint galaxies are obtained using the SExtractor package (Bertin & Arnouts 1996) and detection criteria of 12 WFC pixels above

[6] A fully analytical ray-tracing routine developed by Kneib (1993).

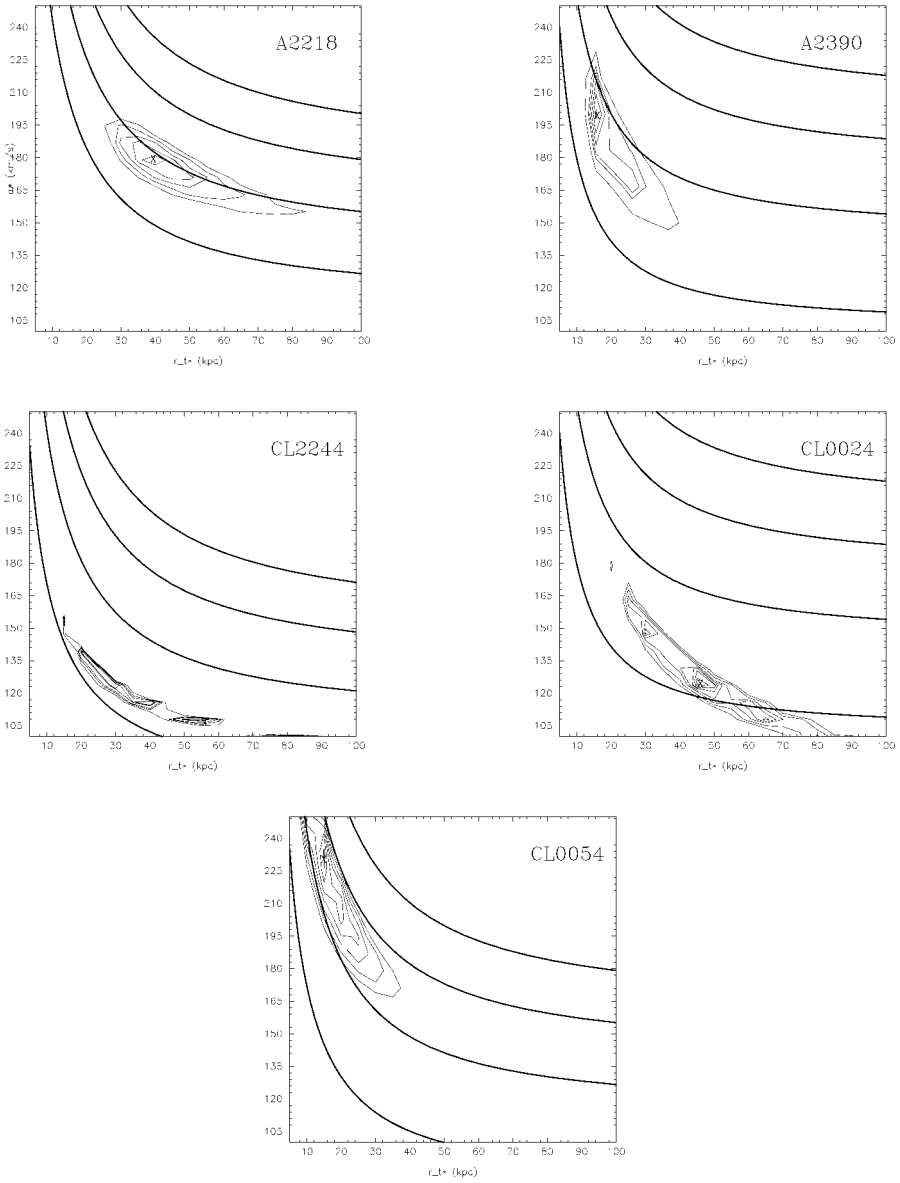

FIG. 1.—Results of the maximum likelihood analysis for the *HST* cluster lenses in our sample; σ^* and r_t^* correspond, respectively, to the central velocity dispersion and the outer scale radius (identified as the tidally truncated radius) for a fiducial L^* cluster galaxy in each of these clusters. The contours start at 1 σ and increase in 1 σ increments from inside out in all five panels. The thick solid lines represent the contours of constant aperture mass, and the best-fit values are marked by the cross.

the μ_R or $\mu_I = 25.0$ mag arcsec^{-2} isophote after convolution with a 0.″3 diameter top-hat filter. Selection of the background galaxies in these images entails a simple magnitude cut that was previously used by NKSE98, either $R = 23$–26 or $I = 22.5$–25.5; this provides catalogs of typically ~300–400 faint galaxies in each field. The magnitude limits employed should select field galaxies at median redshifts of $z \sim 1$, well beyond the clusters. The visual morphological classifications of the brighter galaxies in these fields, used to select the early-type cluster galaxies, come from Smail et al. (1997, 2001).

In addition to the strong lensing model of AC 114 employed by NKSE98, lensing models for three of the other clusters have been published previously: A2218 (Kneib et al. 1996), A2390 (Altieri et al. 1999), and Cl 0024+16 (Smail et al. 1996). For the remaining two lenses, Cl 2244−02 and Cl 0054−27, we construct well-constrained mass models. The mass distribution in Cl 2244−02 has significant substructure, with the main clump centered around the brightest cluster galaxy with a velocity dispersion of 600 ± 80 km s^{-1}, and an ellipticity of 0.17 ± 0.1 and the secondary clump offset about 20″ away with a velocity dispersion of 300 ± 40 km s^{-1} and an ellipticity of 0.1 ± 0.05. By contrast, the cluster Cl 0054−27 has a smooth but extended mass distribution (with a cutoff radius of about 900 ± 60 kpc) with a central velocity dispersion of 1100 ± 100 km s^{-1} and an ellipticity of 0.1 ± 0.05.

4. RESULTS

Before discussing the results, we describe the various tests that we have employed to confirm their reliability. In order to check the authenticity of the signal, the following null tests were performed in the likelihood analysis for every cluster: (1) randomizing the positions of the background galaxies, (2) randomizing the orientations of the background galaxies, and (3) scram-

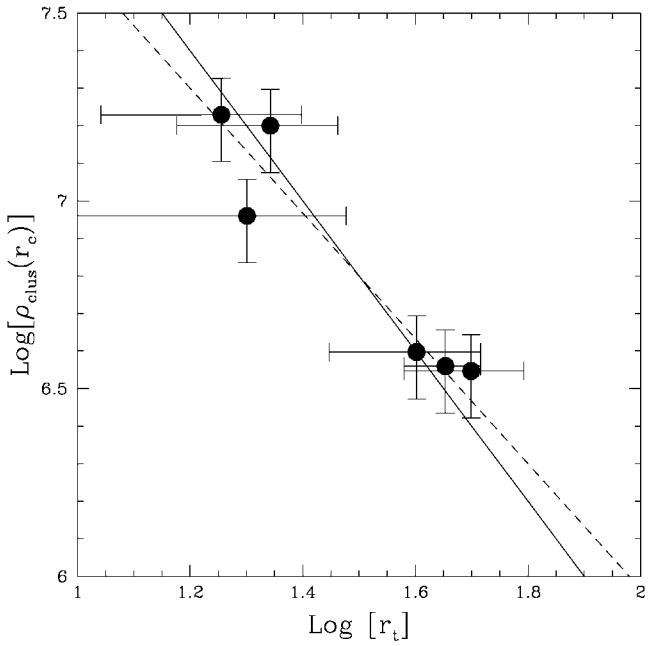

FIG. 2.—Scaling out the variation in the σ^*'s (as per eq. [4]); the central density of the cluster evaluated at the core radius is plotted against the tidal radius. The errors plotted in r_t are the 3 σ values. Performing a least-squares fit to the data points, the value of the best-fit power-law index η, where $r_t^* \propto \rho^\eta$, is estimated to be -0.6 ± 0.2 (*dashed line*), in excellent agreement with theoretical expectations of $\eta = -0.5$ (*solid line*).

bling the positions of cluster galaxies. No significant maxima were obtained in the likelihood prescription for any of these tests in any of the clusters. To quantify the errors on our derived parameters, we note that the principal sources of error in the above analysis are (1) shot noise—we are inherently limited by the finite number of sources sampled within a few tidal radii of each lensing cluster galaxy (in the present analysis, we typically have 40 cluster members and ~400 background sources); (2) the spread in the intrinsic ellipticity distribution of the source population; (3) the unknown source redshifts; and (4) observational errors arising from uncertainties in the measurement of ellipticities from the images for the faintest objects. From simulations in which the detailed mass distribution of clusters is known, we have calibrated the sources of error and find that of the above-mentioned four factors, shot noise (accounts typically for ~50% of the incurred error) and the unknown redshifts for individual background galaxies (contributes ~0%–30% depending on the redshift of the cluster) dominate the error budget. The remaining ~20% of the error budget arises because of inaccuracies in the measurement of shapes.

In Figure 1, we show the likelihood contours for the galaxy perturber models of each of the five clusters. In all cases, we detect an unambiguous galaxy-galaxy lensing signal at greater than 3 σ level, confirming the existence of truncated dark halos associated with early-type galaxies in clusters. The likelihood analysis yields the following best-fit model parameters: the central velocity dispersion σ^* and the truncation radius r_t^* for a typical L^* cluster member; these values are listed in Table 1.[7] The mass-to-light ratios quoted here take the passive evolution of the stellar content of elliptical/S0 galaxies into account, modeled using the stellar population synthesis models of Bruzual & Charlot (1993).

[7] The mass obtained for a typical bright cluster galaxy by Tyson et al. (1984), using only strong lensing constraints inside the Einstein radius of the cluster Cl 0024+16, is consistent with our results.

5. DISCUSSION AND CONCLUSIONS

We have statistically extracted characteristic parameters for typical L^* cluster galaxies that inhabit massive dense lensing cluster lenses ranging in redshift from 0.17 to 0.58. This has been achieved by combining strong and weak lensing *HST* observations in conjunction with an assumed parametric mass model. We find that the inferred mass distribution of a fiducial L^* is extremely compact, although the inferred r_t^*'s lie well outside the optical radii and correspond to roughly between $5R_e$ and $10R_e$. Our analysis also shows that the halos of individual cluster galaxies contribute at most 10%–20% of the total mass of the cluster within the central 1 Mpc, covered by the *HST* WFPC2 imaging using the results of our likelihood analysis along with the best-fit parameters that characterize the smooth clump. Therefore, in the inner regions of these clusters, the bulk of the dark matter is in fact smoothly distributed. Similar lensing studies of field galaxies (e.g., Wilson et al. 2001) typically find a nonzero signal for the radially averaged stacked tangential shear out to 200 kpc. In contrast, our study of halos of galaxies in clusters detects a finite r_t^*, which we attribute to the tidal truncation induced by the motion of these cluster galaxies inside the potential well. From the contours in the likelihood plots, the presence of field galaxy–scale dark halos can in fact be excluded at greater than 10 σ significance.

The clusters that we study here are all rich systems spanning a range in central density, which may explain why the best-fit values of r_t^* obtained vary by a factor of 2–3. To test this suggestion, we plot inFigure 2 the variation of the central density of the cluster dark matter with r_t^*/σ^* based on our lens models and evaluated at the cluster core radius. We see a good correlation and derive a best-fit slope of -0.6 ± 0.2. This compares well with the theoretical expected value from a tidal stripping model (Merritt 1983) of -0.5:

$$r_t^* \approx 40 \left(\frac{\sigma_*}{180 \text{ km s}^{-1}}\right)\left[\frac{\rho_0(r_c)}{3.95 \times 10^6\, M_\odot \text{ kpc}^{-3}}\right]^{-1/2} \text{kpc}. \quad (4)$$

Dark halos of the scale detected here indicate a high probability of galaxy encounters over a Hubble time within a rich cluster. However, since the internal velocity dispersions of these cluster galaxies (<250 km s^{-1}) are much smaller than their orbital velocities, these interactions are unlikely to lead to mergers, suggesting that the encounters of the kind simulated in the "galaxy harassment" picture (Moore et al. 1996) are frequent and likely. In fact, high-resolution cosmological *N*-body simulations of cluster formation and evolution (Ghigna et al. 1998; Moore et al. 1996) show that the dominant interactions are between the global cluster tidal field and individual galaxies after $z = 2$. The cluster tidal field significantly tidally strips galaxy halos in the inner 0.5 Mpc, and the radial extent of the surviving halos is a strong function of their distance from the cluster center. Much of this modification is found to occur between $z = 0.5$ and 0. A detailed comparison of these results with tidal stripping of dark matter halos in cosmological *N*-body simulations will be presented in a forthcoming paper.

The prospects for extending this technique to larger scales within clusters in order to study the efficiency of halo stripping as a function of radius (variation of r_t^* as a function of radius)

and morphological type are very promising with new instruments such as the Advanced Camera for Surveys on *HST*. Multiband imaging will enable us to make photometric redshift determinations for the background sources, and this will reduce one of the significant sources of noise for future analyses.

P. N. acknowledges support from Trinity College, Cambridge, for a Research Fellowship, J.-P. K. acknowledges support from the CNRS and the TMR-Lensing collaboration, and I. S. acknowledges support from the Royal Society and the Leverhulme Trust.

REFERENCES

Altieri, B., et al. 1999, A&A, 343, L65
Bertin, E., & Arnouts, S. 1996, A&AS, 117, 393
Brainerd, T. G., Blandford, R. D., & Smail, I. 1996, ApJ, 466, 623
Bruzual A., G., & Charlot, S. 1993, ApJ, 405, 538
Fischer, P., et al. 2000, AJ, 120, 1198
Geiger, B., & Schneider, P. 1998, MNRAS, 295, 497
Ghigna, S., Moore, B., Governato, F., Lake, G., Quinn, T., & Stadel, J. 1998, MNRAS, 300, 146
Kassiola, A., & Kovner, I. 1993, ApJ, 417, 450
Kneib, J.-P. 1993, Ph.D. thesis, Paul Sabatier Univ.
Kneib, J.-P., Ellis, R. S., Smail, I., Couch, W. J., & Sharples, R. M. 1996, ApJ, 471, 643
McKay, T. A., et al. 2001, preprint (astro-ph/0108013)
Merritt, D. 1983, ApJ, 264, 24
Moore, B., Katz, N., Lake, G., Dressler, A., & Oemler, A. 1996, Nature, 379, 613
Natarajan, P., & Kneib, J.-P. 1997, MNRAS, 287, 833 (NK97)
Natarajan, P., Kneib, J.-P., Smail, I., & Ellis, R. S. 1998, ApJ, 499, 600 (NKSE98)
Okamoto, T., & Habe, A. 1999, ApJ, 516, 591
Smail, I., Dressler, A., Couch, W. J., Ellis, R. S., Oemler, A., Butcher, H., & Sharples, R. M. 1997, ApJS, 110, 213
Smail, I., Dressler, A., Kneib, J.-P., Ellis, R. S., Couch, W. J., Sharples, R. M., & Oemler, A., Jr. 1996, ApJ, 469, 508
Smail, I., Kuntschner, H., Kodama, T., Smith, G. P., Packham, C., Fruchter, A. S., & Hook, R. N. 2001, MNRAS, 323, 839
Smith, D. R., Bernstein, G., Fischer, P., & Jarvis, M. 2001a, ApJ, 551, 643
Smith, G. P., Kneib, J.-P., Ebeling, H., Czoske, O., & Smail, I. 2001b, ApJ, 552, 493
Tyson, J. A., Valdes, F., Jarvis, J. F., & Mills, A. P. 1984, ApJ, 281, L59
Wilson, G., Kaiser, N., Luppino, G. A., & Cowie, L. L. 2001, ApJ, 555, 572